



Published in final edited form as:

IEEE Int Conf Robot Autom. 2015 May ; 2015: 2244–2249. doi:10.1109/ICRA.2015.7139496.

Remote Electromagnetic Vibration of Steerable Needles for Imaging in Power Doppler Ultrasound

Sarah S. Cabrerros*, Nina M. Jimenez*, Joseph D. Greer*, Troy K. Adebar, and Allison M. Okamura

Department of Mechanical Engineering, Stanford University, Stanford, CA 94305 USA

Sarah S. Cabrerros: sarahc08@stanford.edu; Nina M. Jimenez: ninaj2@stanford.edu; Joseph D. Greer: jdgreer@stanford.edu; Troy K. Adebar: tadebar@stanford.edu; Allison M. Okamura: aokamura@stanford.edu

Abstract

Robotic needle steering systems for minimally invasive medical procedures require complementary medical imaging systems to track the needles in real time. Ultrasound is a promising imaging modality because it offers relatively low-cost, real-time imaging of the needle. Previous methods applied vibration to the base of the needle using a voice coil actuator, in order to make the needle visible in power Doppler ultrasound. We propose a new method for needle tip vibration, using electromagnetic actuation of small permanent magnets placed inside the needle to improve needle tip visibility in power Doppler imaging. Robotic needle insertion experiments using artificial tissue and *ex vivo* porcine liver showed that the electromagnetic tip vibration method can generate a stronger Doppler response compared to the previous base vibration method, resulting in better imaging at greater needle depth in tissue. It also eliminates previous issues with vibration damping along the shaft of the needle.

I. Introduction

A. Motivation

Percutaneous procedures allow access to anatomical structures within the body while inflicting minimal trauma to the patient. In clinical practice, application of these procedures may be limited by obstacles or sensitive anatomical structures in proximity to the needle path. Robotically steered needles could allow the clinician to steer around obstacles, correct needle trajectories, and steer to multiple targets during a single insertion. This may allow new procedures to be performed in a percutaneous fashion, while minimizing the invasiveness of existing percutaneous procedures. Robotic needle steering could be widely applicable in clinical practice, for procedures such as biopsy, brachytherapy, and radiofrequency ablation (RFA). For this work, the target application is RFA ablation in the liver.

Image guidance for robotic needle steering systems is critical to the success of these systems in clinical settings. While computed tomography (CT), fluoroscopy and magnetic-resonance imaging all have their own advantages, we focus on ultrasound imaging because it provides

*These authors contributed equally to this work.

real-time imaging of the needle at relatively low cost, and reduces the patient's exposure to ionizing radiation. Despite these advantages, segmentation of needles from ultrasound data is challenging: visibility of the needle is particularly sensitive to transducer-needle orientation, and the images are noisy.

One approach to address these issues is to apply vibration to the needle in tissue, and use the built-in Doppler imaging capability of many modern ultrasound systems to detect the resulting motion. Color and power Doppler images are typically traditional B-mode ultrasound images with overlaid color pixels corresponding to the local velocity of the imaged environment. Prior work demonstrated that high frequency, low-amplitude vibration of the needle creates a visible response in the Doppler ultrasound image that is centered on the needle cross-section in the ultrasound plane [1,2]. The benefits of this response are two-fold: First, the visibility of the needle in the ultrasound image is improved. Second, because the Doppler response serves as a distinct signature highlighting the rough extent of the needle section within the ultrasound image, subsequent image processing required to segment the needle from B-mode data is simplified [3]. Using a combination of B-mode and Power Doppler ultrasound, Greer et al report a needle tip localization error of 0.71 ± 0.27 mm for steerable needles in [3], which is below the maximum targeting error for RFA ablation in the liver suggested in [2]. This paper presents an actuation method for needle tip vibration to further improve the Doppler response consistency of robotically steered needles (Figure 1).

B. Background

1) Needle Vibration—Adebar et al. [2] described a method for generating high frequency, low amplitude needle vibration by attaching a voice coil to the base of a needle. Experiments performed in samples of *ex vivo* bovine liver demonstrated increased needle visibility using this method in comparison to conventional B-mode ultrasound images. However, subsequent tests in the liver of a porcine cadaver resulted in inconsistent power Doppler response. Possible explanations for this inconsistent performance with voice coil base vibration include damping of the vibrations along the length of the needle shaft from the surrounding tissues, damping from the introducer sheath used to access the liver, and lack of ultrasound wave penetration due to gases within the cadaver. To address needle vibration damping, the work presented in this paper investigates direct vibration of the needle tip using remote electromagnetic actuation.

2) Electromagnetic actuation—Electromagnets are an advantageous method of actuation for minimally invasive medical applications because no physical connection between the actuator and the object being moved is required. Relevant examples of this approach include control of untethered micro robots using three concentric solenoids oriented in orthogonal directions surrounding an iron sphere [4], electromagnetic actuation for ocular procedures using eight iron-core solenoids [5], use of an iron-core electromagnet to vibrate ferrous shrapnel in a water bath for visualization in Doppler ultrasound [6], and vibration of brachytherapy seeds in phantom tissue, again to allow visualization in Doppler ultrasound [7].

C. Contributions

Our method combines prior work on needle vibration and electromagnetic actuation to improve ultrasound imaging of flexible needles used in robotic needle steering. An optimized electromagnet configuration remotely actuates permanent magnets inside the needle to cause vibrations that start at the tip and continue along the shaft. This work improves the consistency of the Doppler response due to the vibrations at the needle tip. A consistent Doppler response is necessary for the needle segmentation algorithms described in [2] and [3].

II. Methods

A. Electromagnet Design

100 permanent neodymium magnets (1-mm long, 0.75-mm diameter, N50 magnetic material grade) were placed inside the tip of a hollow needle in order to induce needle vibrations when exposed to an alternating magnetic field.

We developed and tested two configurations of the external electromagnet used to generate the alternating magnetic field. The initial electromagnet configuration was guided by [6], and consisted of a 19.05-mm diameter stainless steel core (a bolt) with 210 turns of 18-gauge magnet wire. An oscillating magnetic field was generated by connecting the coil to an autotransformer, which provided up to 10 A of 60-Hz AC current. This electromagnet successfully generated vibrations of the needle tip, but had several undesirable properties that make it impractical for use in a clinical environment, including sensitivity to bolt position and orientation and excessive heat output.

To guide the design of an improved electromagnet, we performed an optimization of magnetic field strength on a simplified model of the electromagnet. Figure 2 demonstrates the net force and torque of the magnetic field on the needle. Because the net torque, $\vec{\tau}$, on the needle is proportional to the magnetic field strength, $|\vec{B}|$, we chose to maximize $|\vec{B}|$ at a distance of 15 cm from the electromagnet along its axis. The selected distance was chosen as a reasonable estimate of the distance between the needle and the electromagnet during a robotic needle steering procedure.

For an air core solenoid,

$$|\vec{B}| = \frac{\mu_0 N i}{2(r_2 - r_1)l} \left(x_2 \ln \frac{\sqrt{r_2^2 + x_2^2} + r_2}{\sqrt{r_1^2 + x_2^2} + r_1} - x_1 \ln \frac{\sqrt{r_2^2 + x_1^2} + r_2}{\sqrt{r_1^2 + x_1^2} + r_1} \right), \quad (1)$$

where i is the current through the solenoid in amperes, $x_2 = x_1 + l$, μ_0 is the permeability of free space constant ($4\pi \times 10^{-7} \text{N} \cdot \text{A}^{-2}$), N is the number of turns in the coil, and r_1 , r_2 and l are the inner radius, outer radius, and length of the coil respectively (Figure 2).

Electrically, the electromagnet is modeled as a resistor-inductor pair in series. When a sinusoidal voltage source, $v \sin \omega t$, is connected to a resistor-inductor pair in series, the current in the circuit is given by

$$i = \frac{v}{\sqrt{R^2 + L^2 \omega^2}} \cos \omega t, \quad (2)$$

where R is the resistance of the magnetic wire in Ohms and L is the inductance of the electromagnet in Henries. The resistance is due to the coil windings and is given by $R = kl_w$ where k is the resistance per unit length (Ω/m) of the windings and l_w is the length of the magnetic wire, which is an increasing function of N , r_1 , and r_2 . Therefore, maximizing the magnetic field is a constrained optimization problem with constraints given by the maximum voltage, v_{max} , and current, i_{max} , the power supply can support and feasible electromagnet geometry (r_{1min} , r_{1max} , etc.): maximize $r_1 r_2 \cdot l \cdot N \cdot |B|$, subject to $r_{1min} \leq r_1 \leq r_{1max}$, $r_{2min} \leq r_2 \leq r_{2max}$, $i \leq i_{max}$, and $i \sqrt{R^2 + L^2 \omega^2} \leq v_{max}$. This was solved using an exhaustive search over a discretization of the parameter space.

A finite element simulation of the magnetic field was performed to confirm the results from the optimization using the open source software package Finite Element Method for Magnetics (FEMM). The electromagnets were modeled by describing the cross-sectional area of the electromagnet, specifying and defining both the materials and electrical characteristics of the electromagnet. This setup is depicted in Figure 3a. The simulation was defined at 200 Hz to match our experimental setup described below. A 20 cm boundary was defined to perform the finite element analysis, and the mesh size set to 0.1 to control the number of elements. The simulation results are shown in Figure 3. We found the simulation magnetic field strength to be within 10% of the predicted value from the optimization providing confirmation of the results of our optimization. It was calculated that a magnetic field of this magnitude would induce a tip deflection of less than 1 mm in free space, suggesting that the magnetic field magnitude would not induce a dangerous amount of tip deflection in soft tissue.

B. Experimental Setup

The experimental setup consisted of an ultrasound machine and transducer, needle steering robot, Nitinol needles, vibration generation devices (one voice coil actuator and two electromagnets), and tissue simulants (one gelatin and one *ex vivo* porcine liver embedded in gelatin).

1) Ultrasound Imaging—Imaging was performed using a SonixMDP ultrasound console (UltraSonix Medical Corp., Richmond, Canada) and an UltraSonix L14-5/38 GPS Linear transducer. Pulse repetition frequency (PRF) was set to 1.4 kHz, wall motion filter (WF) was set to 157 Hz, and color gain (GainC) was set to 32%. (PRF controls the timing between Doppler pulses, which determines the range of velocities that can be unambiguously resolved; WF removes low frequency Doppler content resulting from slow velocities; GainC controls the brightness of the Doppler data overlaid over B-mode.) These settings were chosen because they resulted in the best Doppler response for each vibration technique while also minimizing Doppler noise.

2) Needle Steering Robot—The robot used to steer our needles is a 2-DOF system that controls needle insertion and rotation (Figure 4). The robot also includes a voice coil

actuator, which is used in one of three needle vibration techniques described in this paper. The robot uses a telescoping sheath to prevent needle bucking [8] and is the same system described in more detail in [2].

3) Needles—The needles were Nitinol tubes with a 0.940-mm outer diameter and 0.787-mm inner diameter. The inner diameter of the needle is constrained by the size of the permanent magnets, but these needle diameter dimensions are close to those used in previous needle steering studies [1,2]. The diameter of the permanent magnets allowed for easy insertion into the needle (Figure 5f). One hundred of the magnets, placed end-to-end, were sufficient to induce significant vibrations of the needle when placed in an alternating magnetic field.

4) Vibration Techniques—In this experiment, three different techniques were used to produce vibration in the needles. These techniques are illustrated in Figures 5c–5e and described below.

Voice coil actuator: The needle steering robot incorporates a voice coil actuator (Figure 5c) driven at a frequency of 600 Hz, which is attached to the base of the needle.

Steel core electromagnet: The steel core electromagnet, previously described, was placed at the surface of the artificial tissue, such that the electromagnet was directly centered on the needle tip. This placement of the electromagnet, shown in Figure 5d, was used in order to remotely vibrate the permanent magnets placed inside the needle. This electromagnet was driven with a 15-A peak-to-peak sinusoidal current at a frequency of 200 Hz.

Air core electromagnet: Like the steel core electromagnet, the air core electromagnet was also placed at the surface of the artificial tissue (Figure 5e) and was directly centered over the needle tip for effective remote vibration. This air core electromagnet was driven with a 5.69-A peak-to-peak sinusoidal current at a frequency of 200 Hz.

Both the steel core and air core electromagnets were driven by a high-current, switching DC power supply. In order to produce an alternating magnetic field, the current for the electromagnets was sourced through a PWM amplifier, driven with a sinusoidal signal from a function generator. Higher frequency currents translate into higher frequency oscillations at the needle tip. Therefore, we wanted as high a frequency as possible. However, electromagnet coil impedance increases linearly with current, hence the frequency of oscillation has to be limited to maintain a strong magnetic field. 200 Hz was found experimentally to balance these two competing factors.

5) Tissue Simulant—This experiment was conducted in two different tissue models. A gelatin mixture with a stiffness of 20 kPa was used for the first tissue model, since its stiffness value is similar to that of human liver [9]. The second tissue model consisted of *ex vivo* porcine liver tissue obtained fresh from a local butcher, which also has been shown to display properties similar to that of human liver [10]. The liver tissue was then set in a gelatin mixture with a stiffness of 20 kPa in order to simulate tissue depth (Figure 5a). A

layer of artificial skin (Figure 5b) was placed in the area where the needles would be inserted to simulate percutaneous procedures.

C. Procedure

The two vibration methods were used in a series of needle insertion tests in an environment designed to simulate the conditions in this procedure. The experiment was first conducted in an artificial tissue simulant, and then repeated in *ex vivo* porcine liver using the setup described above. Starting at one imaging depth, an introducer needle was placed in the tissue and then attached to the needle steering robot. Then, a 0.94-mm needle with magnets placed as described above was inserted into the tissue at four 2-cm increments. At each increment, the needle was vibrated in place using the voice coil, air core electromagnet, and stainless steel core electromagnet. The electromagnets were placed in the position and orientation as described in Section II.B.4. The ultrasound transducer was placed on top of the tissue and tilted so that the ultrasound image plane was perpendicular with the needle axis. Next, power Doppler was enabled, and the PRF and WF were set as described in Section II.B.1. The average Doppler response over a series of twenty consecutive images was recorded. At the maximum insertion depth, the needle was vibrated with a constant magnet position while Doppler images were recorded at eight 1-cm increments along the shaft of the needle. This process for shaft imaging was repeated for all three vibration techniques. After completing this, the needle was retracted and then reinserted to repeat the procedure for each of the four imaging depths. Figure 6 shows a diagram of the procedural setup and the values used in the experiment.

III. Results

Experimental results in both the gelatin tissue phantom and *ex vivo* porcine liver demonstrated the strong performance of the new electromagnet method in power Doppler ultrasound imaging. To quantify Doppler response, the sum of Doppler pixel intensity was averaged over a series of image frames. This metric was chosen because it represents the strength and consistency of Doppler response produced by each vibration method. Similar metrics have been used to quantify total Doppler response in past blood perfusion studies [11]. Figures 7a and 7b track the Doppler response of the three different vibration methods at the tip of the needle as it is inserted into the gelatin tissue phantom and *ex vivo* porcine liver respectively. At the maximum imaging depth of 8 cm, the air core electromagnet had the strongest Doppler response for all insertion lengths. In addition, the voice coil generated a Doppler response at the tip of the needle that generally decreased as the needle was inserted further into the tissue. The steel core electromagnet produced the least amount of Doppler response. The same test in *ex vivo* porcine liver resulted in similar trends. However, in liver the voice coil generated less Doppler response than both electromagnets.

Figures 8a and 8b display the trends in Doppler response for each method at different imaging depths, focusing at a fixed 12 cm needle insertion length. Each method is plotted along imaging depth, and a logarithmic scale was used to display total Doppler response. In both the artificial tissue and the *ex vivo* porcine liver, there is a decreasing trend in Doppler response for all three methods as the imaging depth increases. At the smallest imaging depth, the air core and steel core electromagnets generate similar Doppler responses;

however, as imaging depth increases, the air core electromagnet produces a strong Doppler response than the steel core electromagnet. Across all the imaging depths, the voice coil produces the least amount of Doppler response compared to both electromagnets.

Figures 9a and 9b display the relationship between Doppler response and the imaging location along the shaft of the needle. This data is taken from a fixed 12-cm needle insertion depth and fixed 4-cm imaging depth. In both the artificial tissue and *ex vivo* porcine liver, the voice coil Doppler response decreases as the imaging location moves from the base of the needle towards the tip. This decreasing trend is due to the imaging location moving further from the vibration source as it is swept from base to tip. For both the air core and steel core electromagnets, the Doppler response is relatively low along the shaft of the needle until the imaging location reaches the needle tip, where there is a sudden drastic increase. This increasing trend is due to the imaging location moving closer to the source of vibration in the needle. These opposite trends highlight a key difference between voice coil vibration at the base and magnetic vibration at the tip.

IV. Needle Reconstruction Based on Electromagnetically induced vibration

To demonstrate the applicability of electromagnet-induced vibration to 3D reconstruction of steerable needles, the needle described in Section II.B was embedded in a polyvinyl chloride rubber phantom and vibrated using the air core electromagnet also described in Section II.B. A power Doppler volume of the phantom tissue surrounding the needle was captured with a convex mechanical 3D transducer (model 4DC7-3/40, Ultrasonix Medical Corp., Richmond, Canada). The needle shape was reconstructed by fitting a polynomial to the centroids of the Doppler patches of the individual volume slices, similar to the techniques described in [2] and [3]. A visualization of the ultrasound volume and 3D reconstruction is shown in Figure 10.

V. Discussion

The results from experiments in artificial tissue and *ex vivo* porcine liver demonstrate the effective use of electromagnets to vibrate a needle for visualization in Doppler ultrasound imaging. Compared to the previous method of voice coil base vibration, our results show that the electromagnetic tip method can produce more consistent Doppler responses at the needle tip as it is inserted further. These results support the possibility that the base vibrations from the voice coil can be dampened by the tissue itself before reaching the tip.

Comparing the two electromagnet configurations, the data shows that the air core electromagnet generates a larger Doppler response than the steel core at greater imaging depths. In these cases, the electromagnet is farther away from the needle tip, and the air core electromagnet has a farther reaching magnetic field than the steel core electromagnet. This reaffirms the results of the optimization methods discussed previously which were used to increase the magnetic field range of the air core electromagnet.

Our results also suggest the effectiveness of the electromagnetic vibration for localization of the needle tip, as opposed to the entire needle shaft. As demonstrated in Figure 9, the Doppler response is very low until the imaging plane is near the tip of the needle, where

there is a significant increase in Doppler response. The increasing trend of Doppler response provides a clear indication of when the ultrasound transducer has passed over the needle tip. This is in contrast to the Doppler response due to the voice coil vibration, which tends to have a decreasing trend of Doppler response moving from the proximal to the distal end of the needle.

The embedded permanent magnets occupy the entire hollow space of the needle tip, however this not problematic for our intended application, radiofrequency (RFA) ablation, as the needle itself can be used as an RFA probe. Furthermore, the needle may be used as a guidewire for other devices. On the other hand, the effect of the embedded magnets on the needle's steerability will need to be studied in the future, though it appeared to be minor. Finally, safety considerations will need to be addressed in future work such as subjecting the body to both the time varying magnetic field and heat generated by the electromagnet before it can be successfully used in a clinical environment.

Acknowledgments

This work is supported in part by National Institute of Health Grant #R01EB01884901

The authors thank Kelly Lowen, Caroline Fong, Sanjay Srinivas, and Ann Majewicz for their contributions.

References

1. Fronheiser MP, Idriss SF, Wolf PD, Smith SW. Vibrating interventional device detection using real-time 3-D color Doppler. *IEEE Trans Ultrason Ferroelectr Freq Control*. Jun; 2008 55(6):1355–1362. [PubMed: 18599423]
2. Adebar TK, Fletcher AE, Okamura AM. 3-D Ultrasound-Guided Robotic Needle Steering in Biological Tissue. *IEEE Transactions on Biomedical Engineering*. Dec.2014 61(12):2899, 2910. [PubMed: 25014948]
3. Greer JD, Adebar TK, Hwang GL, Okamura AM. Real-time 3D curved needle segmentation using combined B-Mode and power Doppler ultrasound. *Medical Image Computing and Computer-Assisted Intervention*. 2014:381–388. [PubMed: 25485402]
4. Petruska, AJ.; Abbott, JJ. An omnidirectional electromagnet for remote manipulation. *IEEE International Conference on Robotics and Automation*; 2013. p. 822-827.
5. Kummer MO, Abbott JJ, Kratochvil BE, Borer R, Sengul A, Nelson BJ. OctoMag: An electromagnetic system for 5-DOF wireless micromanipulation. *IEEE Transactions on Robotics*. 2010; 26(6):1006–1017.
6. Rogers AJ, Light ED, Smith SW. 3-D ultrasound guidance of autonomous robot for location of ferrous shrapnel. *IEEE Transactions on Ultrasonics, Ferroelectrics, and Frequency Control*. 2009; 56(7):1301–1303.
7. McAleavey SA, Rubens DJ, Parker KJ. Doppler ultrasound vibration of magnetically vibrated brachytherapy seeds. *IEEE Transactions on Biomedical Engineering*. 2003; 50(2):252–255. [PubMed: 12665040]
8. Webster, Robert J.; Memisevic, Jasenka; Okamura, Allison M. Design considerations for robotic needle steering. *IEEE International Conference on Robotics and Automation*. 2005:3588–3594.
9. Nava A, Mazza E, Furrer M, Villiger P, Reinhart WH. In vivo mechanical characterization of human liver. *Medical Image Analysis*. 2008; 12:203–216. [PubMed: 18171633]
10. Ocal S, Ozcan MU, Basdogan I, Basdogan C. Effect of preservation period on the viscoelastic material properties of soft tissues with implications for liver transplantation. *Journal of Biomechanical Engineering*. 2010; 132(10):101007.1–7. [PubMed: 20887017]

11. Chen, Chiung-Nien, et al. Association of color Doppler vascularity index and microvessel density with survival in patients with gastric cancer. *Annals of surgery*. 2002; 235(4):512. [PubMed: 11923607]
12. Yesin K, Berk K, Vollmers K, Nelson BJ. Modeling and control of untethered biomicrobots in a fluidic environment using electromagnetic fields. *The International Journal of Robotics Research*. 2006; 25(5–6):527–536.
13. Griffiths, DJ. *Introduction to Electrodynamics*. Englewood Cliffs, NJ, USA: Prentice-Hall; 1999.

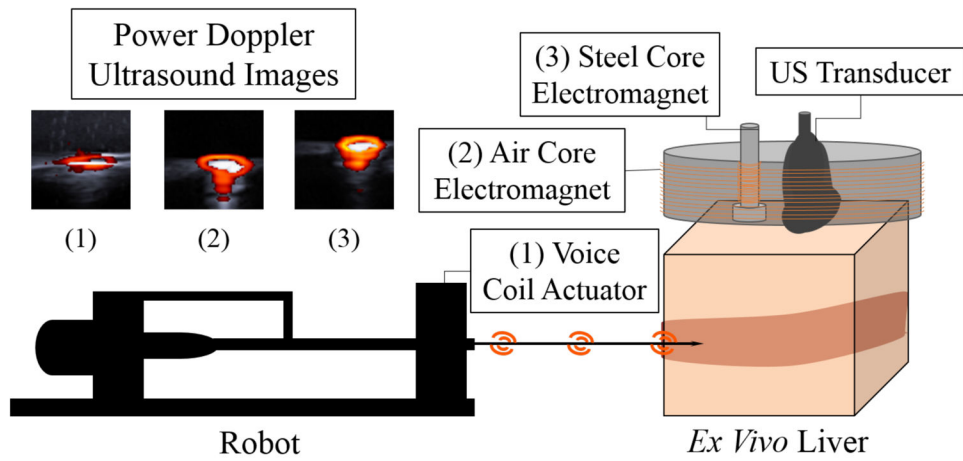


Figure 1. Three needle vibration methods that provide enhanced needle visibility in ultrasound imaging via Doppler ultrasound: (1) voice coil actuator, (2) air core electromagnet, and (3) steel core electromagnet.

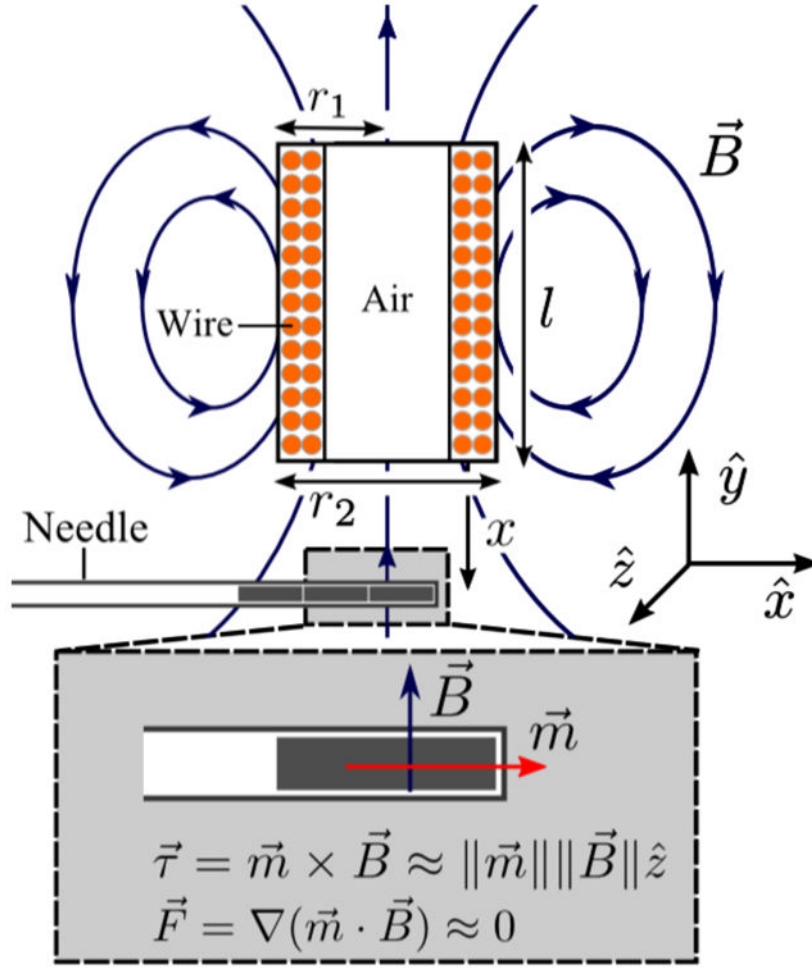


Figure 2. Conceptual overview of electromagnetic actuation of the needle tip. The magnetic field generated by the electromagnet, \vec{B} , and the magnetic moments of the permanent magnet in the needle tip, \vec{m} , are approximately perpendicular, simplifying the calculation of net force, F , and torque on the permanent magnets, τ , due to the magnetic field of the electromagnet.

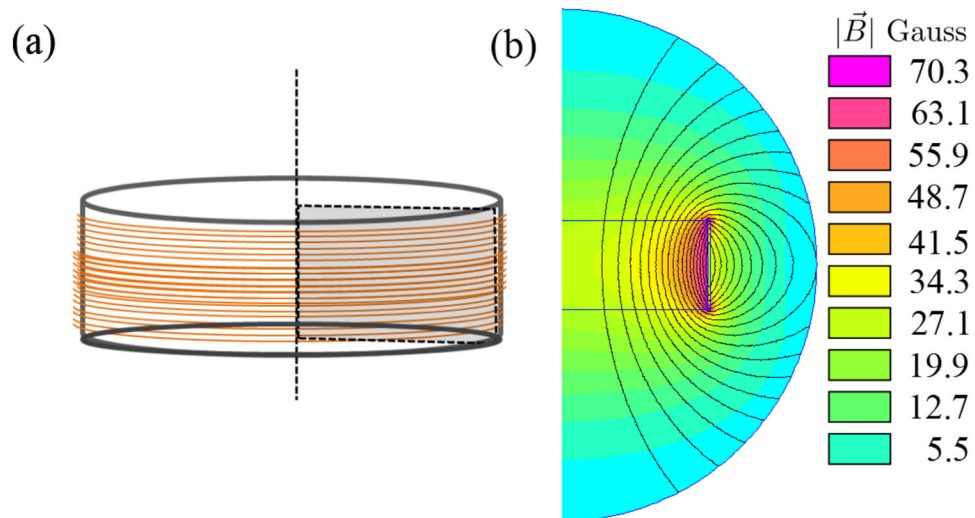


Figure 3.

(a) Diagram of the air core electromagnet simulated in FEMM, which was used to verify the predicted magnetic field that resulted from the optimization procedure. (b) Output from FEMM. The simulation output consisted of a contour density map of the magnitude of magnet field density in Gauss. The entire magnetic field within a radius of 20 cm of the center of the electromagnet was calculated in the simulation using the geometry and parameters of the electromagnet: 23-cm radius, 7-cm length, 96 turns of wire in the coil, and 200-Hz frequency, 5.69-A peak-to-peak sinusoidal current through 18-gauge magnet wire.

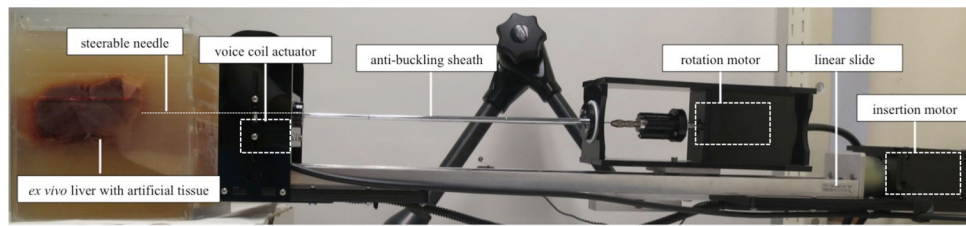


Figure 4. Experimental setup. A needle steering robot, consisting of insertion and rotation motors, a linear slide, an anti-buckling sheath, and a voice coil actuator, inserts a steerable needle into *ex vivo* porcine liver and artificial tissue.

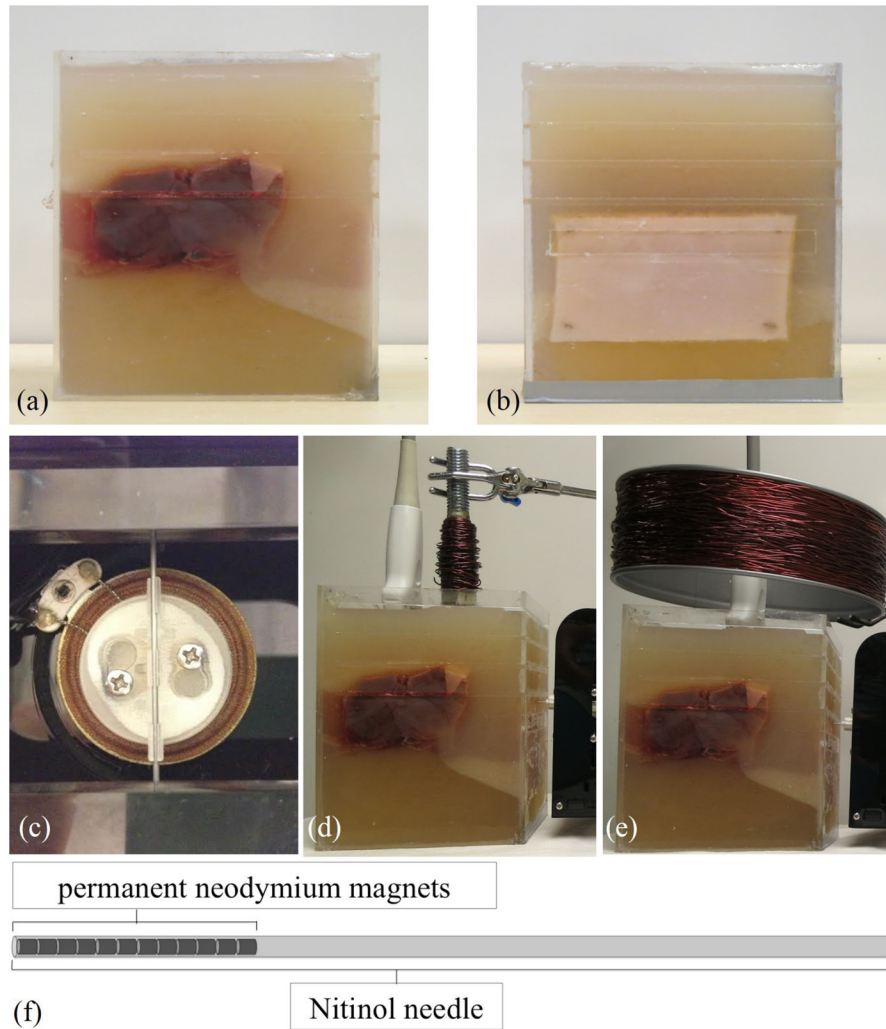


Figure 5. Components of experimental setup. (a) *Ex vivo* porcine liver set in gelatin. (b) Layer of skin simulant at needle insertion area. (c) Voice coil actuator with needle attachment. (d) Steel core electromagnet and ultrasound transducer. (e) Air core electromagnet and ultrasound transducer. (f) Diagram of Nitinol needle with removable permanent neodymium magnets placed inside needle tip.

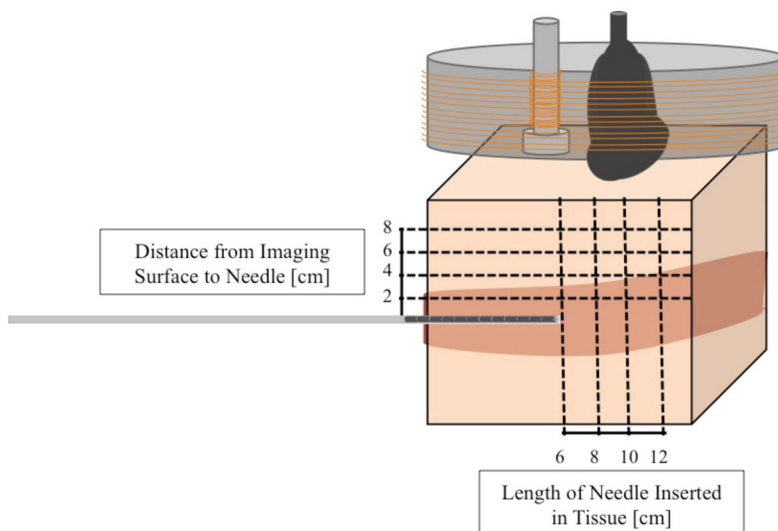


Figure 6. Locations for measurement of needle power Doppler response. For each imaging depth (2 cm to 8 cm), the needle was incrementally inserted to a maximum length of 12 cm. At each insertion increment, a Doppler response was measured at the tip using the power Doppler imaging mode of the ultrasound machine. Finally, when the needle reached an insertion length of 12 cm, the Doppler response was measured along the needle’s shaft, starting at the tip and moving to the base.

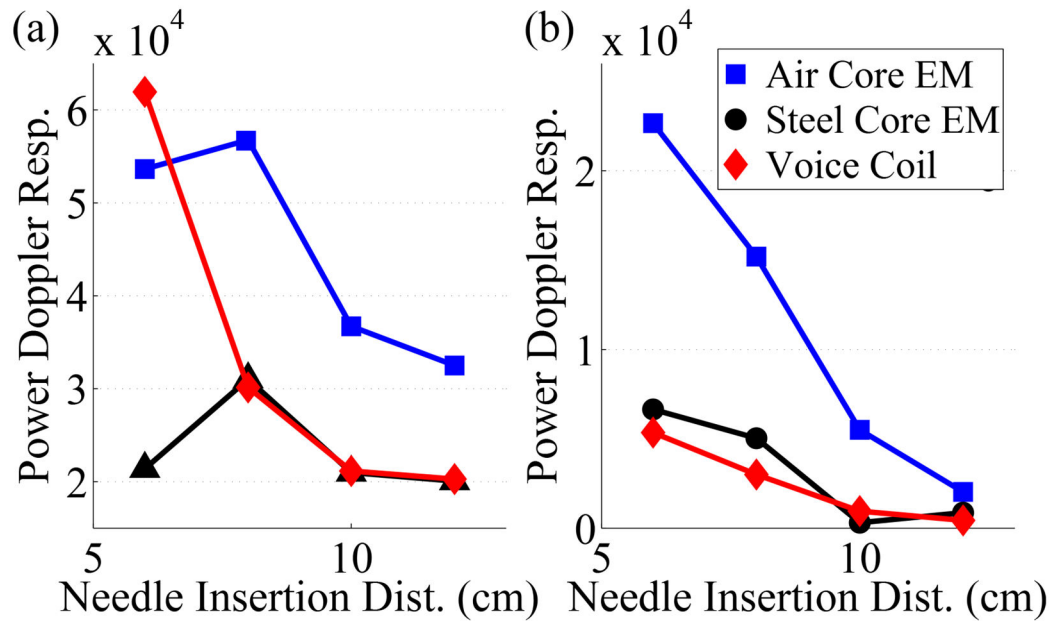


Figure 7. Doppler response of needle tip in (a) artificial tissue and (b) *ex vivo* porcine liver with varying needle insertion lengths (6–12 cm) and fixed imaging depth (8 cm). In both artificial tissue and *ex vivo* liver, the air core electromagnet produces the strongest Doppler response. Both artificial tissue and *ex vivo* liver data also show that the steel core electromagnet and voice coil produce similar Doppler response (except at 6 cm insertion depth in artificial tissue), weaker than that of the air core electromagnet.

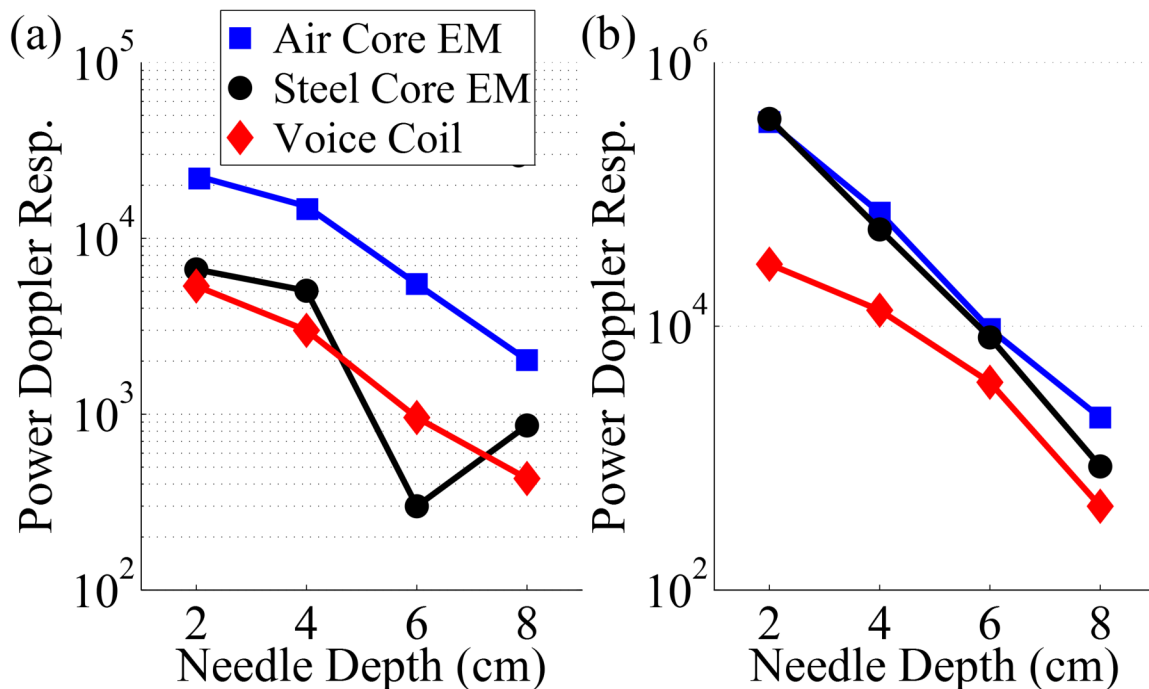


Figure 8. Doppler response at the needle tip with varying imaging depths and fixed needle insertion length (maximum insertion of 12 cm) in (a) artificial tissue and (b) ex vivo porcine liver. Note that the response is plotted on a logarithmic scale. In both artificial tissue and *ex vivo* liver, the air core electromagnet produces the strongest Doppler response at all imaging depths. Both artificial tissue and *ex vivo* liver data also show that the steel core electromagnet produces the second strongest Doppler response, while the voice coil produces the weakest Doppler response out of all three vibration techniques.

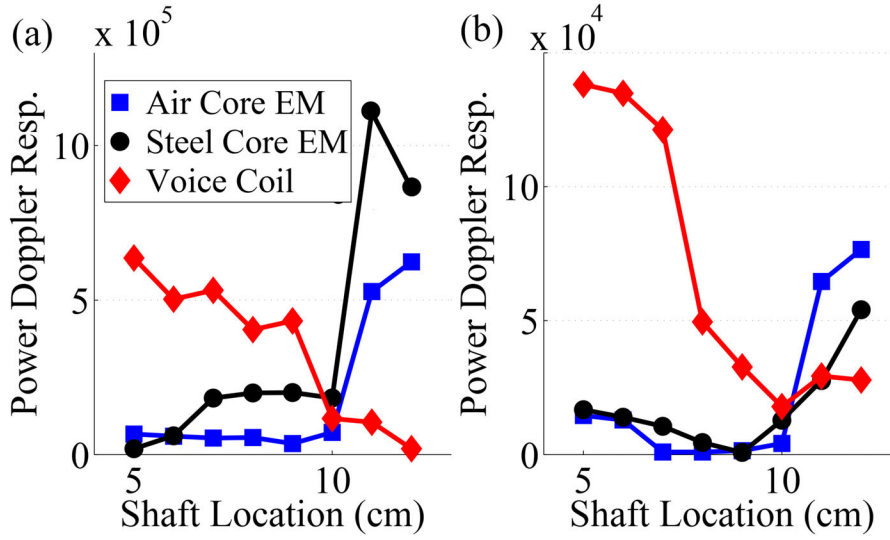


Figure 9. Doppler response at various points along the needle shaft at a fixed imaging depth (4 cm) in (a) artificial tissue and (b) *ex vivo* porcine liver. Both artificial tissue and *ex vivo* liver data show that the voice coil’s Doppler response has a generally decreasing trend when moving from the base of the needle to the tip. In contrast, both the air core and steel core electromagnets show a generally increasing trend in Doppler response when moving from the needle base to the tip. These results also show that both electromagnets allow for better localization of the needle tip compared to the voice coil.

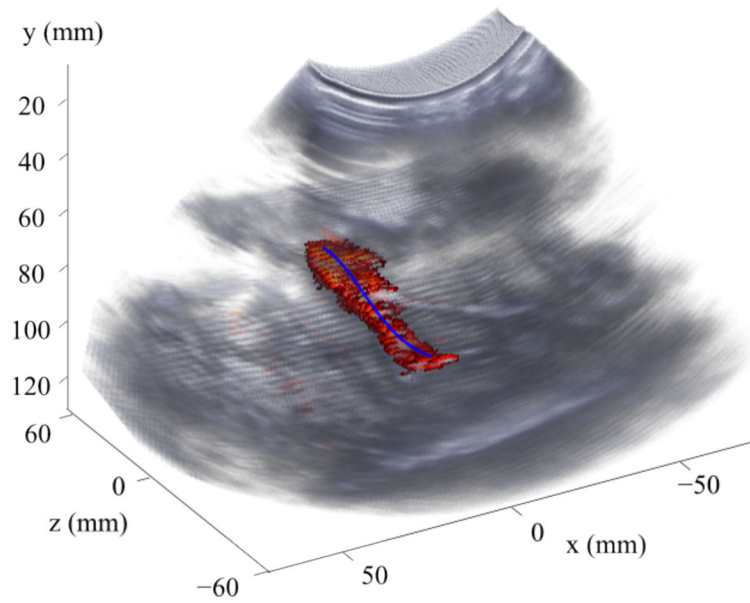


Figure 10.

3D reconstruction of a steerable needle generated using the Doppler response to magnetic vibration of the steerable needle. The surrounding B-mode data is visualized in black and white, the Doppler response in orange, and the reconstructed needle in blue.